4.5 The July 12, 1993 Hokkaido-Nansei-Oki tsunami

The Hokkaido Nansei-Oki earthquake occurred on July 12, 1993, at13:17 GMT with the epicenter located at 42.851˚ N and 139.197˚ E approximately 50*km* off the Hokkaido west coast in the vicinity of a small island of Okushiri. The surface wave magnitude was 7.6 according to the National Earthquake Information Center. The tsunami generated by this earthquake produced in Japan the worst local tsunami-related death toll in fifty years (Shuto and Matsutomi, 1995), with measured 30*m*-high wave runup. These extreme values are the largest recorded in Japan this century and are among the highest ever documented for non-landslide generated tsunamis.

The estimation of the moment magnitude of this earthquake by different agencies varies from $M_w = 0.93$ of USGS to $M_w = 6.3$ of JMA (To. Takahashi et al., 1995[1]); the fault parameters has also been estimated very diversely. These differences suggest significant complexity of the source mechanism of this earthquake which occurred on the recently recognized boundary between the Eurasian and North American plates. A discussion of the seismological aspects of the source mechanism of tsunami is out of the scope of the present study; the source mechanism and associated tsunami source of this event are discussed by To. Takahashi et al. (1995) and by Satake and Tanioka (1995). In this tsunami application and for reference with the other existing simulations; the three–fault plane dipole–shaped ground deformation model of To. Takahashi et al (1995) referred to as DCRC–17 will be used as the initial condition (Figure 4.44). DCRC–17 predicts a maximum uplift of 4.2*m*

1. The initial of To. Takahashi is included because there are two papers written about this event. The other is by T. Takahashi

and subsidence of 1.1*m* and it has produced the closest qualitative agreement with the field observations to date among different source models (Myers and Baptista, 1995; Satake and Tanioka, 1995; To. Takahashi et al., 1995).

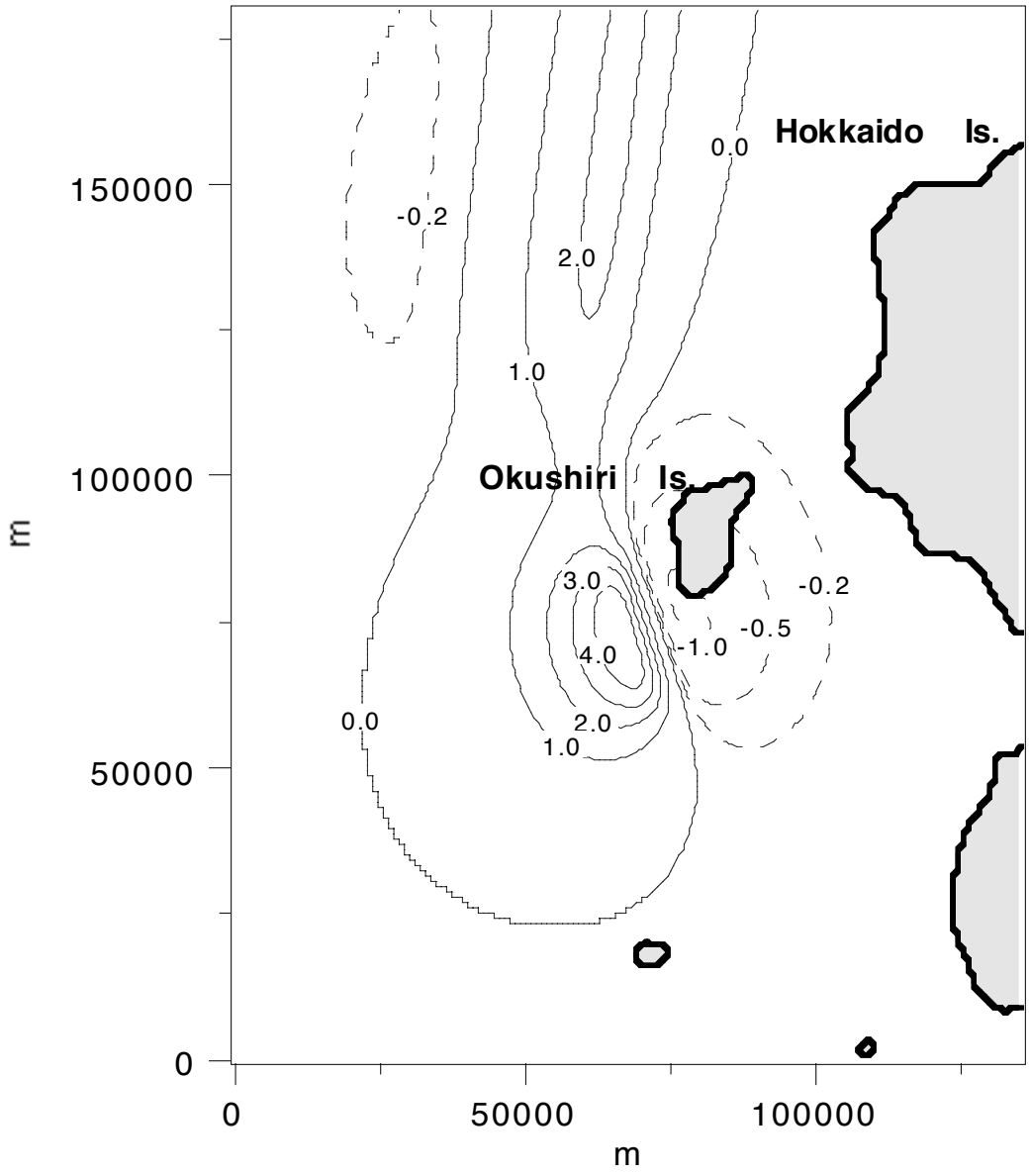

Figure 4.44 Contours of the sea-bed displacement of the source model DCRC-17 of the Hokkaido-Nansei-Oki earthquake.

For the tsunami scientists, the Hokkaido–Nansei–Oki earthquake can be considered as a fortuitous large–scale experiment which allowed the measurement of high quality run-up data and the inference of fairly unambiguous ground deformation contours due to its proximity to seismic instrument arrays. At the same time, high–resolution bathymetry data are available, allowing not only the evaluation of the predictive capabilities of the VTCS-3 model for extreme events and the effects of the 10*m*–depth calculation threshold and of topography resolution limits, but also the relative effects of inundation heights and inundation–flow velocities.

Hydrodynamic computations reported to date (Myers and Baptista, 1995; Satake and Tanioka, 1995; To. Takahashi et al., 1995) using the SW approximation demonstrated that the hydrodynamic models are able to reproduce to first–order the general patterns of the runup heights distribution along the coast of Hokkaido and to some extent around Okushiri, but they were unable to reproduce wave current velocities and the extreme runup values observed in the front of the island; at best (To. Takahashi et al., 1995*)*, predictions have not differed significantly from the field data, but they have been unable to reproduce the extreme measured runup heights of 30*m* or the large overland current velocities.

The digitized bathymetry for our numerical experiments was generously provided by the Disaster Control Research Center in Tohoku University to formulate benchmark problem number 4 for the International Long Wave Runup Workshop discussed in the introduction. It consists of several nested bathymetric arrays with three levels of grid resolution. The main array contains the area of computation with grid size of 450*m* and covers a

large area of the Sea of Japan including the source area, Okushiri Island and the west coast of Hokkaido Island. The coast of Okushiri island is covered by 7 nested arrays with grid 150*m* and 50*m*. For the locations where 50*m* grid is available, i.e. in Aonae and Monai areas see (figure 4.35), computations using all three available resolutions of the bathymetry were performed to investigate the influence of the spatial grid size on the results.

Figure 4.35 shows the distribution of the computed runup heights around Okushiri using VTCS–3 and it compares them with the field measurements (Hokkaido Tsunami Survey Group, 1993; Shuto and Matsutomi, 1995). The computed distribution of the maximum runup heights reproduces most features of the field measurements well. The extreme 31.7*m* measurement near Monai was computed as 29.7*m*. The measurement was made at the tip of a small canyon and it is undoubtedly a local effect; yet all measurements around it were consistently high with a global maximum at 31.7*m*, similar to the distribution of computed values shown in the figure.This suggests that this high runup measurement was not the result of only local inland topography, but also the effect of the small scale nearshore bathymetry, such as several small islands close to the shore. Most computed runup values are slightly higher than measured, but then this model does not include any dissipation. The largest difference is near Inaho at the north, where the calculations predict 15*m* heights compared to the 10*m* field measurements (Hokkaido Tsunami Survey Group, 1993); interestingly, 12-15*m* field measurements have been reported at Inaho by other Japanese reconnaissance teams *(*Nakasuji T. and Takahashi, 1993). Overall, for this extreme tsunami event the SW model appears adequate for modeling runup heights, suggesting that wave breaking and bottom friction are apparently not important to first–order for predicting inundation.

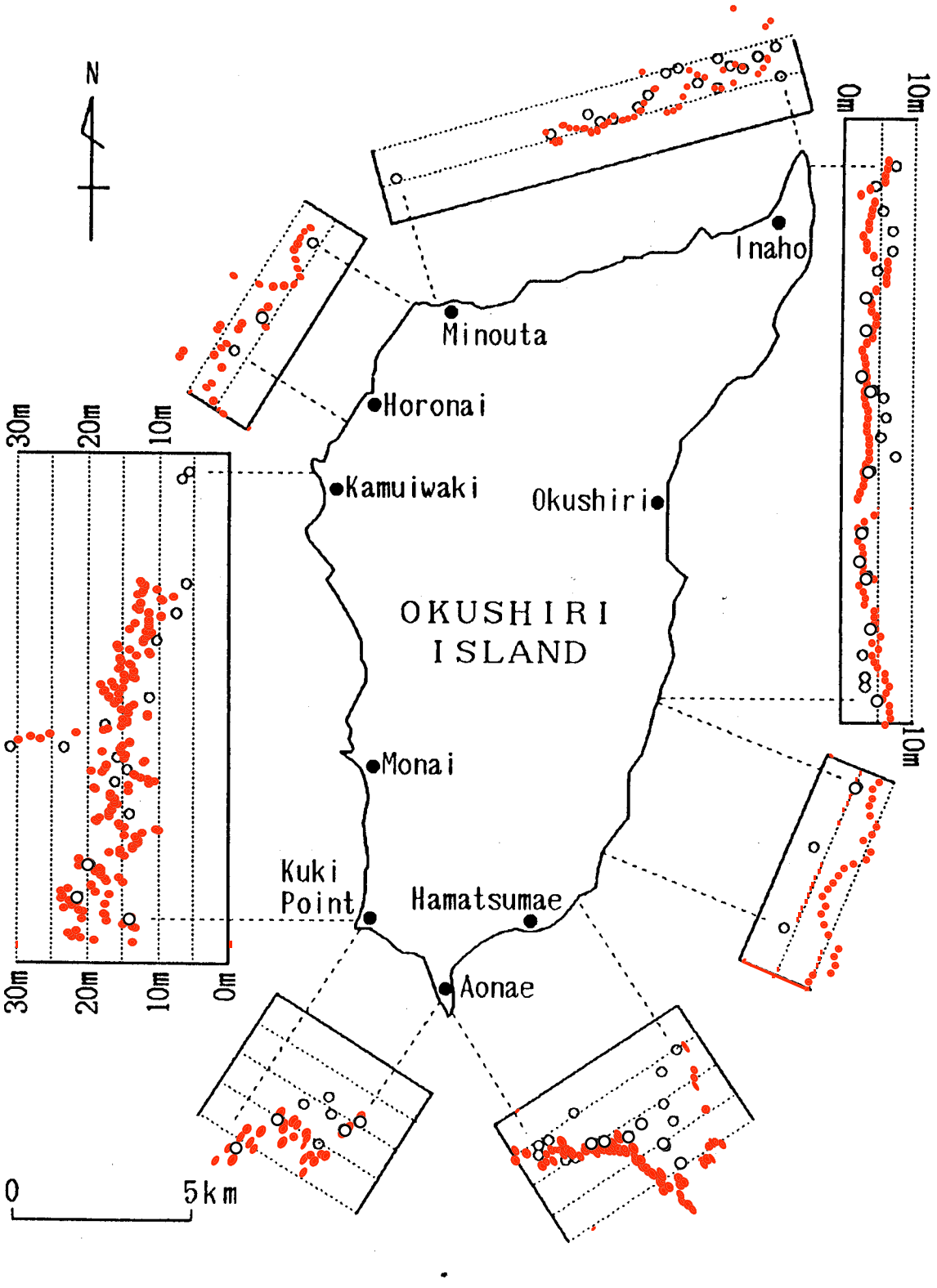

Figure 4.45 Comparison of the computed runup heights with field measurements.

Another challenging computation for the SW theory is overland flow, a condition referring to waves overtopping a peninsula or a narrow strip of land sandwiched between the ocean and a tidal inlet, then propagating over it and then draining on the lee side of the land. Overland flow has been identified (C. E. Synolakis et al., 1995) as one of the leading causes of the heavy casualties during tsunami attack because of the high flow velocities. During tsunami runup on a sloping beach, the shoreline front slows down as its kinetic energy is converted into potential energy, but during overland flow over flat land the kinetic energy is only reduced by dissipation. Overland flow is usually supercritical with bore–like dynamics.

Overland flow results near Aonae are presented in the three flow snapshots of Figure 4.46, before, during and after the overland flow. The dynamics are very similar to those inferred from the field observations (Hokkaido Tsunami Survey Group, 1993; T. Shimamato et al., 1995). Eyewitnesses reported that south part of the peninsula was flooded by the first wave which came from the west and overtopped the south cape, the computations suggest similar dynamics, as seen in Figure 4.46. The east part of Aonae was flooded later by the wave from the east, this process was also reproduced by the model. The boundaries of the flooded area is computed very close to the measured boundaries at this location. The snapshot of flow velocities during the overland flow shown in Figure 4.47 suggests values in the range of 10-19m/s over the Aonae peninsula, consistent with the 10-18m/s field estimates of in Aonae (T. Shimamato, 1995).

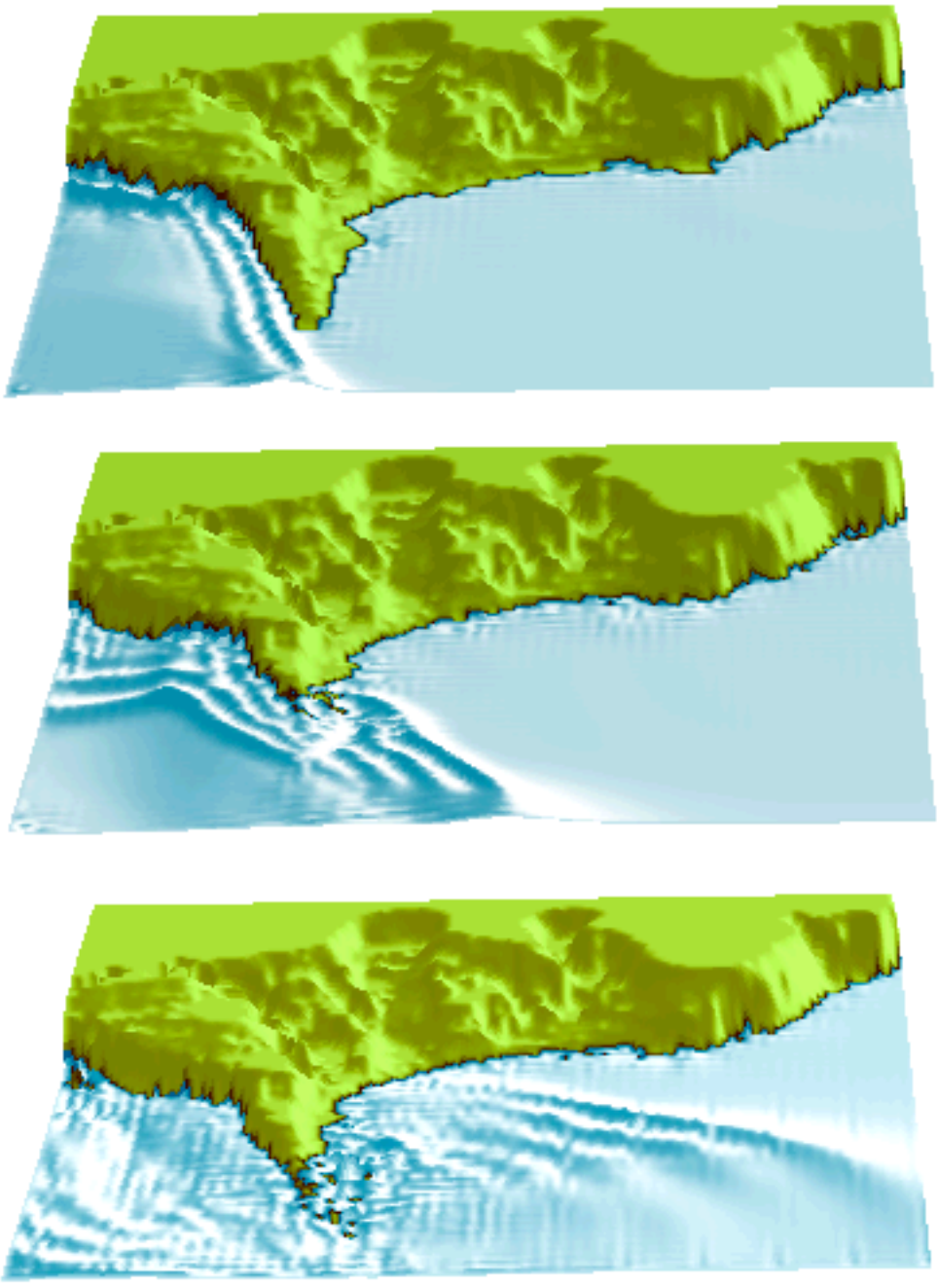

Figure 4.46 Bird-eye views of the computed tsunami wave overflowing Aonae cape after 310 sec of propagation from the source, 375 sec and 500 sec. The horizontal scale is the same as in Figure 4.47.

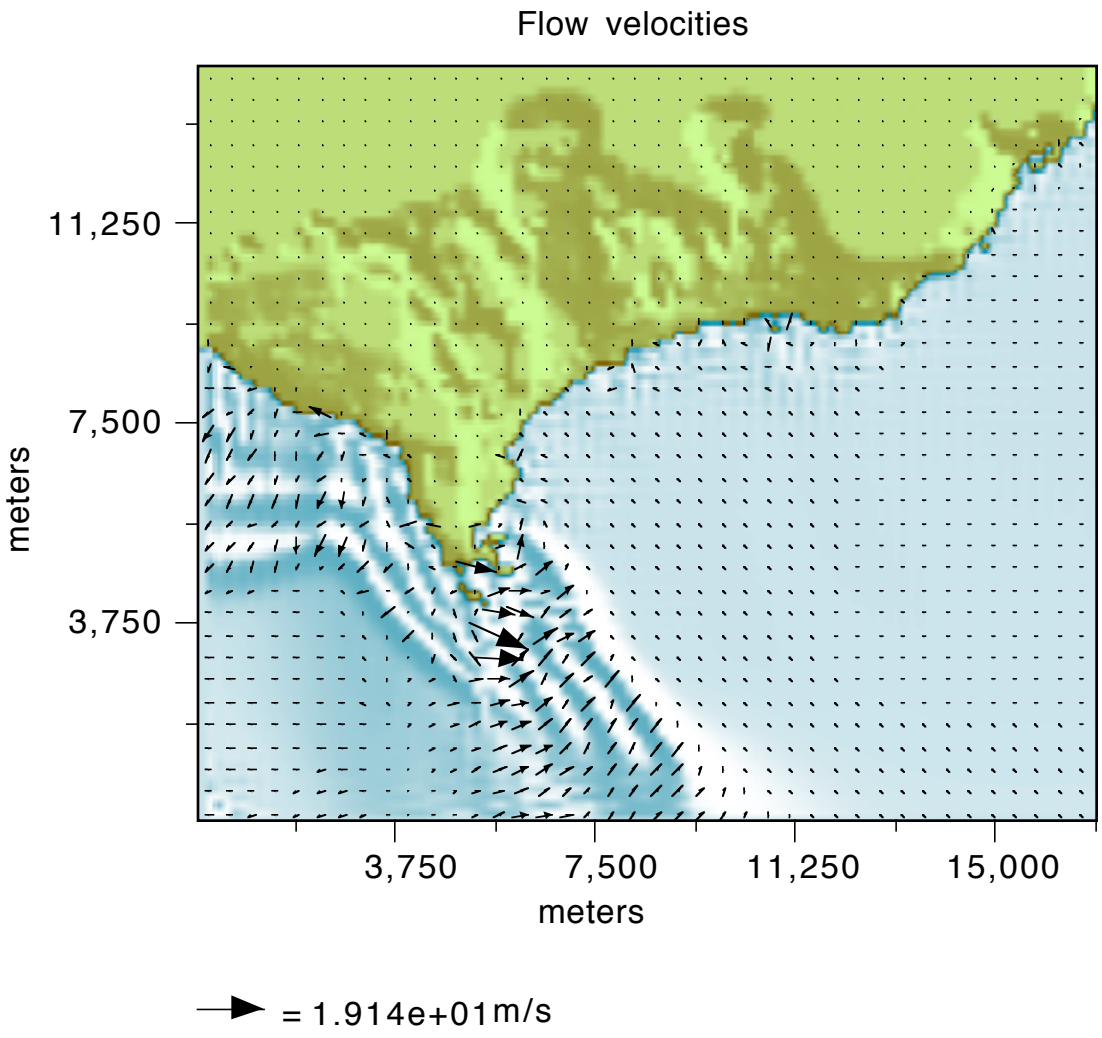

Figure 4.47 Flow-velocities distribution during overland flow in Aonae 375 sec after the tsunami generation. The instantaneous inundation boundary is also shown.

Figure 4.48 shows the envelope of maximum tsunami heights and of maximum wave velocities over one typical topographic cross-section of Aonae cape. Notice that the highest inundation velocities occur at the east side of Aonae where inundation heights are smallest, and the extreme velocities correlate well with the most devastated area. This is

entirely consistent with the fact that the during the lee–side rundown of the overland flow, the flow depths are small, but the flow is supercritical with large flow velocities, and it underlines the risk of relying exclusively on runup heights to predict inundation.

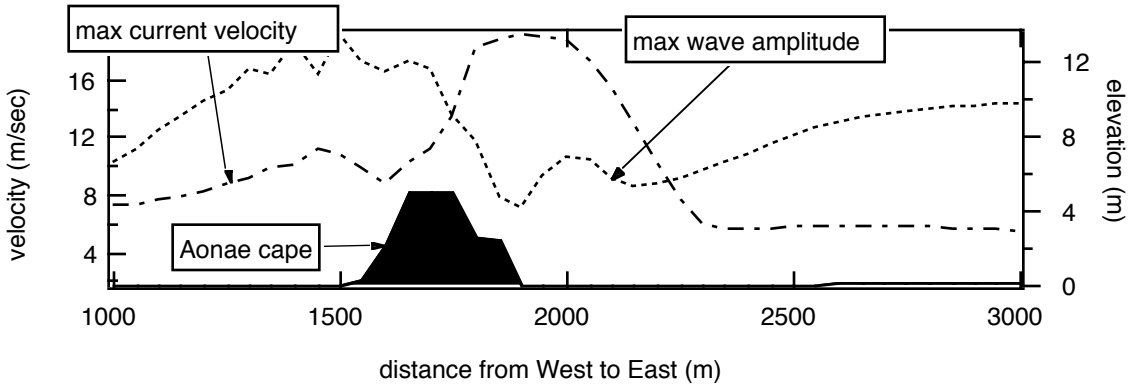

Figure 4.48 Computed envelope of maximum tsunami heights and of maximum wave velocities over one topographic cross-section of Aonae cape

To further illustrate the significance of the flow velocities for the estimation of the tsunami inundation, we computed the distribution of the maximum velocities around Aonae. Figure 4.49 shows contours of the maximum computed velocities along with the maximum computed inundation line. We found that the contour line of $5m/s$ maximum velocities correlates approximately with zones of violent destruction during the tsunami inundation. Note the low–velocity (less than $5m/s$) area on the right (east) shore of Aonae cape. This location was protected by higher elevation ground from the first wave that came from the west and caused overflow on the southern part of the cape. The area was flooded by the second wave that came from the east. The aerial photograph on Figure 4.50 suggests that flooded houses in this location did not suffer substantial damage, although right next to

these houses on the south is the area of complete devastation where the overflow with high velocities swept away all construction.

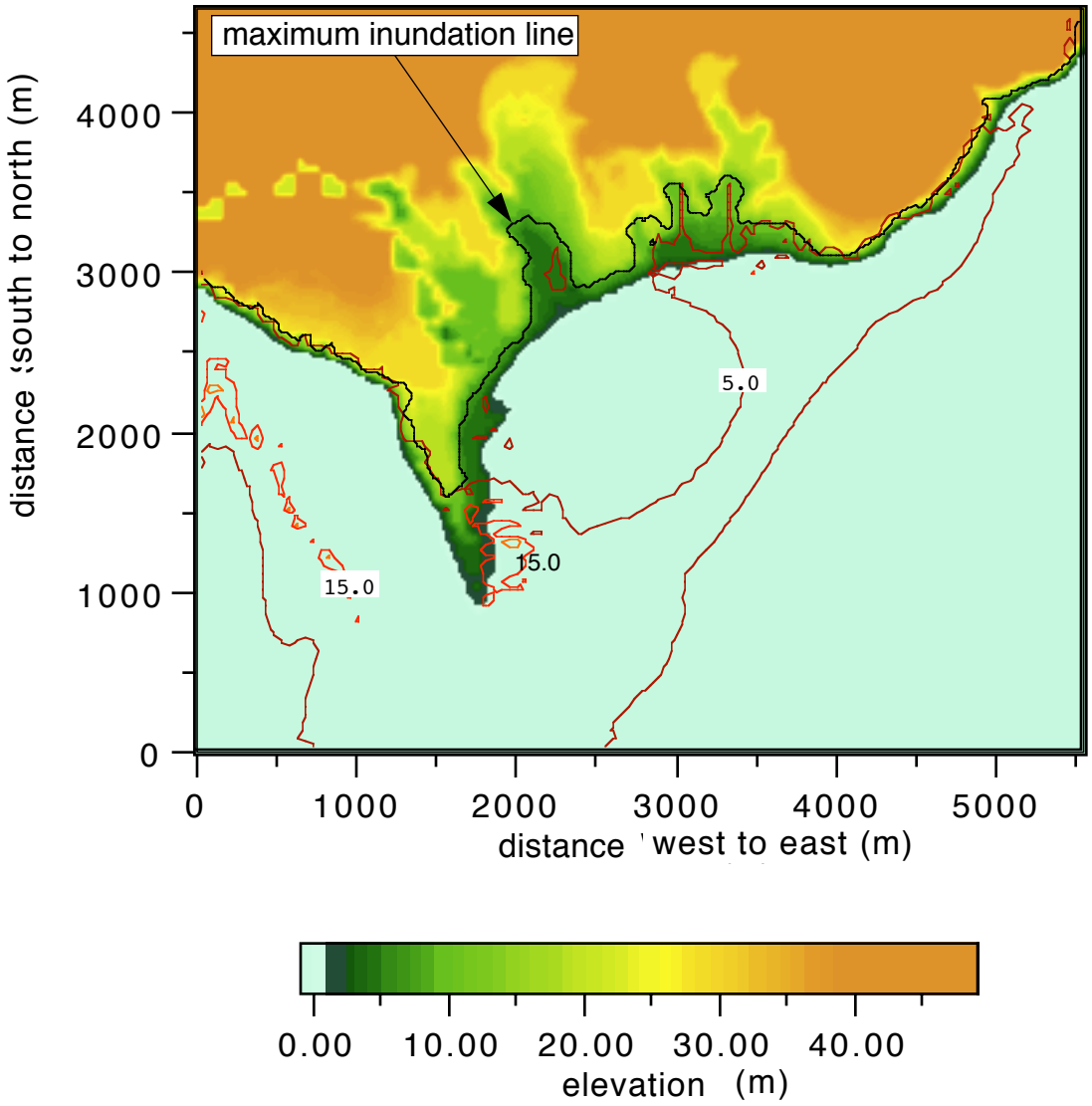

Figure 4.49 Contours of computed maximum flow velocities (*m/s*) over the Aonae cape area. Computed maximum inundation line is also shown on top of the topographic map.

Figure 4.50 The aerial photograph of the tsunami devastation on the Aonae peninsula. The picture was taken the day after the Hokkaido-Nansei-Oki earthquake[1].

The contour of 15*m*/*sec* velocities indicates the area of extremely high velocities occurred during the overland flow on the east shore of Aonae cape. The other location of over 15*m*/*sec* velocities along the west coast of the Aonae cape marks the area of high velocities during the water withdrawal. The maximum run-down velocities were computed near the

1. Courtesy of Mamoru Takahashi, Kokusai Kogyou Co.

line of the furthest water recession after the first wave. In this location the water-line receded down to 10m depth which is distant 500m to 700m from the original shoreline. No witness confirmation of this result was found published anywhere, possibly because the tsunami occurred during night time. Numerous witness accounts of such distant water withdrawal during several other tsunami events indirectly support the computed estimates.

A series of numerical experiments was performed to evaluate the effect of other aspects of numerical modeling, such as the grid resolution and the 10m-depth threshold. Figure 4.51 compares runup results among computations with different grid resolutions for a region of the west coast of Okushiri island where topographic data exist down to 50m-square resolution. For reference, the leading N-wave close to the shoreline (Tadepalli and Synolakis, 1995) has a $O(1km)$ wavelength, and therefore the computations shown range from 3-4 points per wavelength for the 450m grid to 20 points per wavelength for the 50m grid. The computations with the 150m grid produce qualitatively correct runup distribution, but miss the extreme runup height. The computations with the 450m grid, even though adequate in terms of hydrodynamic stability to resolve the waveform (Titov and Synolakis, 1995), they seriously underpredict the runup height, suggesting that it is the effect of the small-scale features hidden in the coarse grid and not only the effect of wavelength resolution. This is rather important, as problems arising only from wavelength resolution can be solved easily by generating denser grids through interpolation of the coarser grid, yet these denser grids have identical topography resolutions as the coarse grids that produced them.

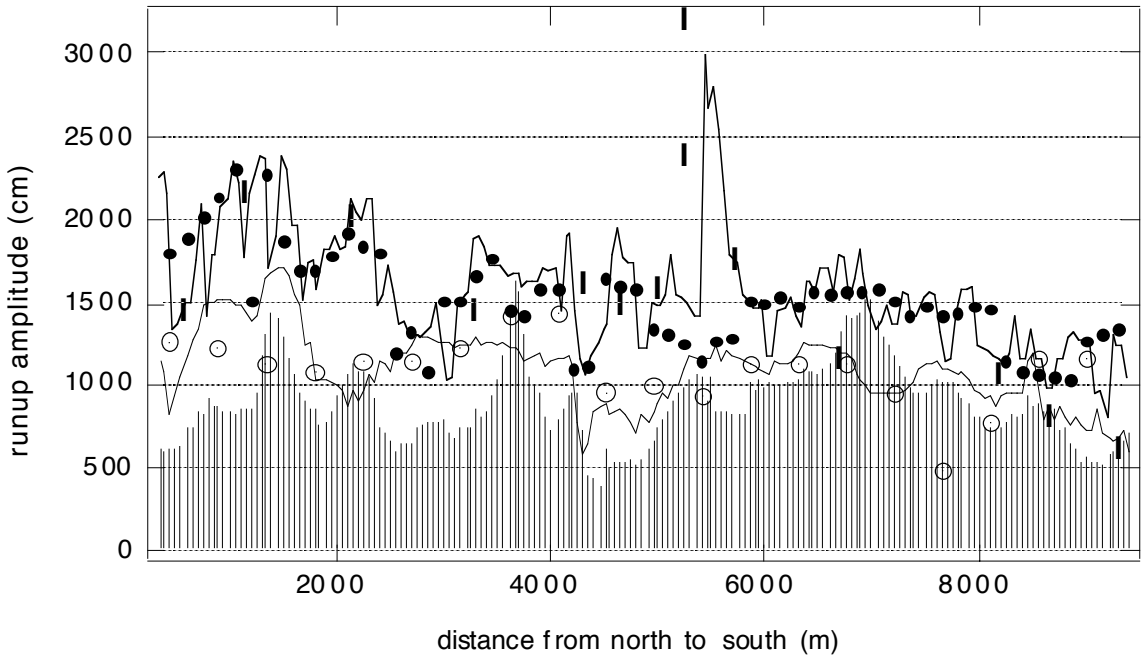

Figure 4.51 Comparison of the computed runup heights among computations using different grid resolutions and different types of computations thresholds. The heavy line, the solid circles and the empty circles are model predictions including inundation computations using a 50*m*, a 150*m* and a 450*m* grid respectively. The vertical bars are inferred runup height using a 10*m*-depth threshold in the 50*m* grid calculation, i.e., the wave height at the 10*m* depth if a vertical wall was there. The thin line is the maximum wave height at the 10*m*--depth contour for the 50*m* grid inundation computations. Stars are the runup measurements (from Shuto and Matsutomi, 1995).

Figure 4.51 also present results from numerical experiments to compare the predictions of models with 10*m*-contour calculation thresholds. These models are still ubiquitous (Yeh, et al.,1993; Synolakis et al.,1995; Satake and Tanioka,1995) and they propagate the wave using a SW model up to the 10*m* contour, and then use the maximum wave height at that location to infer the maximum runup height. It has been argued repeatedly, that these models are probably adequate for civil defense computations. For identical grid resolutions,

the results show that interrupting the computation at the 10*m* depth, a step essentially equivalent to placing reflective "wall"-type boundaries at that depth, underpredicts the runup by a factor of two, as compared with the inundation computations. Even the computed maxima at the 10*m* contour from the full inundation calculation differ substantially from the computed maxima from the 10*m*-threshold "wall" calculations, suggesting that this latter practice needs to be re-evaluated. Clearly the wave evolves substantially as it propagates from the 10*m* depth up the beach to its maximum runup.

The simulation shows that the described solution method is capable of modeling quantitatively correctly tsunami inundation, including extreme runup heights and inundation velocities. It is found that even small local bathymetric structures affect inundation, and therefore predictions are limited by coarse topographic resolution which may hide local features. Also, it appears that coastal devastation correlates stronger with inundation velocities than inundation heights.